The Cryosphere Discuss., https://doi.org/10.5194/tc-2019-22
Manuscript under review for journal The Cryosphere
Discussion started: 20 February 2019

The Cryosphere Discussions

Inter-comparison and improvement of 2-stream shortwave radiative transfer models for unified treatment of cryospheric surfaces in ESMs

Cheng Dang[1], Charles S. Zender[1], Mark G. Flanner[2]

[1] Department of Earth System Science, University of California, Irvine, CA, USA
[2] Department of Climate and Space Sciences and Engineering, University of Michigan, Ann Arbor, MI, USA

Correspondence to: Cheng Dang (cdang5@uci.edu)

Abstract. Snow is an important climate regulator because it greatly increases the surface albedo of large parts of the Earth. Earth System Models (ESMs) often adopt 2-stream approximations with different radiative transfer techniques, the same snow therefore has different solar radiative properties depending whether it is on land or on sea ice. Here we inter-compare three 2-stream algorithms widely used in snow models, improve their predictions at large zenith angles, and introduce a hybrid model suitable for all cryospheric surfaces in ESMs. The algorithms are those employed by the SNow ICe and Aerosol Radiative (SNICAR) module used in land models, and by Icepack, the column physics used in the Los Alamos sea ice model CICE and MPAS-seaice, and a 2-stream discrete ordinate (2SD) model. Compared with a 16-stream benchmark model, the errors in snow visible albedo for a direct-incident beam from all three 2-stream models are small (<±0.005) and increase as snow shallows, especially for aged snow. The errors in direct near-infrared (near-IR) albedo are small (<±0.005) for solar zenith angles $\theta < 75°$, and increase as θ increases. For diffuse incidence under cloudy skies, Icepack produces the most accurate snow albedo for both visible and near-IR (<±0.0002) with the lowest underestimate (-0.01) for melting thin snow. SNICAR performs similarly to Icepack for visible albedos, with a slightly larger underestimate (-0.02), while it overestimates the near-IR albedo by an order of magnitude more (up to 0.04). 2SD overestimates both visible and near-IR albedo by up to 0.03. We develop a new parameterization that adjusts the underestimated direct near-IR albedo and overestimated direct near-IR heating persistent across all 2-stream models for solar zenith angles > 75°. These results are incorporated in a hybrid model SNICAR-AD, which can now serve as a unified solar radiative transfer model for snow in ESM land, land ice, and sea-ice components.

The Cryosphere Discuss., https://doi.org/10.5194/tc-2019-22
Manuscript under review for journal The Cryosphere
Discussion started: 20 February 2019

1. Introduction

Snow cover on land, land ice, and sea ice, modulates the surface energy balance of large parts of the Earth, principally because even a thin layer of snow greatly increases the surface albedo. Integrated over the solar spectrum, the broadband albedo of opaque snow ranges from 0.7 – 0.9 (e.g., Wiscombe and Warren 1980; Dang et al., 2015). In contrast, the albedo of other natural surfaces is smaller: 0.2, 0.25, and 0.5-0.7 for damp soil, grassland, and bare multi-year sea ice, respectively (Perovich 1996; Liang et al., 2002; Brandt et al., 2005; Bøggild et al., 2010). An accurate simulation of the shortwave radiative properties of snowpack is therefore crucial for spectrally partitioning solar energy and representing snow-albedo feedbacks across the Earth system. Unfortunately, computational demands and coupling architectures often constrain representation of snowpack radiative processes in Earth System Models (ESMs) to relatively crude approximations such as 2-stream methods (Wiscombe and Warren, 1980, Toon et al., 1989). In this work, we inter-compare 2-stream methods widely used in snow models and then introduce a new parameterization that significantly reduces their snowpack reflectance and heating biases at large zenith angles, to produce more realistic behavior in polar regions.

Snow albedo is determined by many factors including the snow grain radius, the solar zenith angle, cloud transmittance, light-absorbing particles, and the albedo of underlying ground if snow is optically thin (Wiscombe and Warren, 1980; Warren and Wiscombe, 1980); it also varies strongly with wavelength since the ice absorption coefficient varies by 7 orders of magnitudes across the solar spectrum (Warren and Brandt, 2008). At visible wavelengths (0.2 - 0.7 μm), ice is almost non-absorptive so that the absorption of visible energy by snowpack is mostly due to the light-absorbing particles (e.g. black carbon, organic carbon, mineral dust) that were incorporated during ice nucleation in clouds, scavenged during precipitation, or slowly sedimented from the atmosphere by gravity (Warren and Wiscombe, 1980, 1985; Doherty et al., 2010, 2014, 2016; Wang et al., 2013; Dang and Hegg 2014). As snow becomes shallower, visible photons are more likely to penetrate through snowpack and get absorbed by darker underlying ground. At near-infrared (near-IR) wavelengths (0.7 – 5 μm), ice is much more absorptive and the snow albedo is lower than the visible albedo. Larger ice crystals form a lower albedo surface than smaller ice crystals hence aged snowpacks absorb more solar energy. Photons incident at smaller solar zenith angles are more likely to penetrate deeper vertically and be scattered in the snowpack until being absorbed by the ice/the underlying ground/absorbing impurities, which also leads to a smaller snow albedo. To compute the reflected solar flux, spectrally resolved albedo must be weighted by the incident solar flux, which is mostly determined by solar zenith angle, cloud cover and transmittance, and column water vapor. Modeling the solar properties of snowpacks must consider the spectral signatures of these atmospheric properties.

Several parameterizations have been developed to compute the snow solar properties without solving the radiative transfer equations and some are incorporated into ESMs or regional models. Marshall and Warren (1987) and Marshall (1989) parameterized snow albedo in both visible and near-IR bands as functions of snow grain size, solar zenith angle, cloud transmittance, snow depth, underlying surface albedo, and black carbon content. Marshall and Oglesby (1994) used this in an ESM. Gardner and Sharp (2010) parameterized the all-wave snow albedo with similar inputs. This was incorporated into the regional climate model RACMO (https://www.projects.science.uu.nl/iceclimate/models/racmo.php) to simulate snow albedo in glaciered regions like Antarctica and Greenland (Munneke et al., 2011). Dang et al., (2015) compute snow albedo as functions of snow grain radius, black carbon content, and dust content for visible and near-IR bands and 14 narrower bands used in the rapid radiative transfer model (RRTM, Mlawer and Clough, 1997). Their parameterization can also be expanded to different solar zenith angles using the zenith angle parameterization developed by Marshall and Warren (1987). Aoki et al., (2011) developed a more complex model (PBSAM) based on the offline snow albedo and a transmittance look-up table. This can be applied to multilayer snowpack to compute the snow albedo and the solar heating profiles as functions of snow grain size, black carbon and dust content, snow temperature, and snowmelt water equivalent. These parameterizations are often in the form of simplified polynomial equations, and are especially suitable to long-term ESM simulations that require less time-consuming snow representations.

More complex models that explicitly solve the multiple scattering radiative transfer equations have also been developed to compute snow solar properties. Flanner and Zender (2005) developed the SNow Ice and Aerosol Radiation model (SNICAR) that utilizes 2-stream approximations (Wiscombe and Warren 1980; Toon et al., 1989) to predict heating and reflectance for multi-layer snowpack. They implemented SNICAR in the Community Land Model (CLM) to predict snow albedo and vertically-resolved solar absorption for snow-covered surfaces. Before SNICAR, CLM prescribed snow albedo and confined all solar absorption to the top snow layer (Flanner and Zender 2005). Over the past decades, updates and new features have been added to SNICAR to consider more processes such as black carbon/ice mixing states (Flanner et al., 2012) and snow grain shape (He et al., 2018b). Concurrent with the development of SNICAR, Briegleb and Light (2007) improved the treatment of sea-ice solar radiative calculations in Community Climate System Model (CCSM). They implemented a 2-stream delta-Eddington method that allows CCSM to compute bare/ponded/snow-covered sea ice albedo and solar absorption profiles of multi-layer sea ice. Before these improvements, the sea-ice albedo was computed based on surface temperature, snow thickness, and sea-ice thickness using averaged sea ice and snow albedo. This method has carried into the sea-ice physics library Icepack (https://github.com/CICE-Consortium/Icepack/wiki) that comprises the column physics used by the Los Almos Sea Ice Model CICE (Hunke et al., 2010) and MPAS-seaice (Turner et al., 2018). CICE itself is used in numerous global and regional models.

The shortwave methods in SNICAR and in CICE solve the multiple scattering radiative transfer equations and provide much improved solar radiative representations for the cryosphere, though their separate development and implementation created an artificial divide for snow simulation. In ESMs that utilize both SNICAR and CICE/MPAS-seaice, such as the Community Earth System Model (CESM, http://www.cesm.ucar.edu/) and the Energy Exscale Earth System Model (E3SM, previously known as ACME, https://e3sm.org/), the solar radiative properties of snow on land and snow on sea ice are computed separately via SNICAR and CICE/MPAS-seaice. As a result, the same snow in nature has different solar radiative properties such as reflectance depending on which model represents it. These differences are model artifacts that should be eliminated so that snow has consistent properties across the Earth system.

In this paper, we evaluate the accuracy and biases of three 2-stream algorithms described in Section 2 and Table 1, including the algorithms used in SNICAR and Icepack, at representing reflectance and heating. We use these results to develop and justify a unified surface shortwave radiative transfer method for all Earth system model components in the cryosphere.

2. Radiative Transfer Model

In this section, we summarize the three 2-stream models and the benchmark DISORT

The Cryosphere Discuss., https://doi.org/10.5194/tc-2019-22
Manuscript under review for journal The Cryosphere
Discussion started: 20 February 2019

model with 16-streams. These algorithms are well documented in papers by Toon et al., (1989), Briegleb and Light (2007), Jin and Stamnes (1994), and Stamnes et al. (1988). Readers interested in detailed mathematical derivations should refer to those papers. We only include their key equations to illustrate the difference among 2-stream models for discussion purposes.

2.1 SNICAR

SNICAR adopts the 2-stream algorithms and the rapid solver developed by Toon et al., (1989) to compute the solar properties of multi-layer snowpacks. These 2-stream algorithms are derived from the general equation of radiative transfer in a plane parallel media:

$$\mu \frac{\partial I}{\partial \tau}(\tau,\mu,\Phi) = I(\tau,\mu,\Phi) - \frac{\varpi}{4\pi}\int_0^{2\pi}\int_{-1}^{1} P(\mu,\mu',\phi,\phi')\, I(\tau,\mu',\Phi')d\mu' d\phi' - S(\tau,\mu,\Phi) \tag{1}$$

where arccos(μ) and Φ are zenith angle and azimuth angle, ϖ is single-scattering albedo. On the right-hand side, the three terms are intensity at optical depth τ, internal source term due to multiple scattering, and external source term S. For a purely external source at solar wavelengths S is:

$$S = \frac{\varpi}{4} F_s P(\mu,-\mu_0,\phi,\phi_0) exp\left(\frac{-\tau}{\mu_0}\right) \tag{2}$$

where πF_s is incident solar flux, μ_0 is the incident direction of the solar beam. Integrating equation (1) over azimuth and zenith angles yields the general solution of 2-stream approximations (Meador and Weaver, 1980). The upward and downward fluxes at optical depth τ of layer n can be represented as:

$$F_n^+ = k_{1n}\, exp(\Lambda_n\tau) + \Gamma_n k_{2n}\, exp(-\Lambda_n\tau) + C_n^+(\tau) \tag{3a}$$

$$F_n^- = \Gamma_n k_{1n}\, exp(\Lambda_n\tau) + k_{2n}\, exp(-\Lambda_n\tau) + C_n^-(\tau) \tag{3b}$$

where Λ_n, Γ_n C_n are known coefficients determined by the 2-stream method, incident solar flux, and solar zenith angle; whereas k_{1n} and k_{2n} are unknown coefficients

The Cryosphere Discuss., https://doi.org/10.5194/tc-2019-22
Manuscript under review for journal The Cryosphere
Discussion started: 20 February 2019

The Cryosphere Discussions
Open Access

determined by the boundary conditions. For an N-layer snowpack, the solutions for upward and downward fluxes are coupled at layer interfaces to generate 2N equations with 2N unknown coefficients k_{1n} and k_{2n}. Combining these equations linearly generates a new set of equations with terms in tridiagonal form that enables the application of a fast tri-diagonal matrix solver. With the solved coefficients, the upward and downward fluxes are computed at different optical depths (Equations 3a and 3b) and eventually the reflectance, transmittance, and absorption profiles of solar flux for any multilayer snowpack.

SNICAR itself implements all three 2-stream algorithms in Toon et al., (1989): Eddington, Quadrature, and Hemispheric-mean. In ESM simulations, it utilizes the Eddington and Hemispheric-mean approximations to compute the visible and near-IR snow properties, respectively (Flanner et al., 2007). In addition to their algorithms, SNICAR implements a Delta-transform of the fundamental input variables asymmetry factor (g), single-scattering albedo (ϖ), and optical depth (τ) to account for the strong forward scattering in snow (Equations 2 (a)-(c), Wiscombe and Warren, 1980).

2.2. Icepack, CICE, and MPAS-seaice

Icepack, CICE and MPAS-seaice use the same solar radiative treatment developed and documented by Briegleb and Light (2007). In the following discussions, we will refer to this method as CICE since it is more widely used. Sea ice is divided into multiple layers to first compute the single-layer reflectance and transmittance using 2-stream delta-Eddington solutions to account for the multiple scattering of light within each layer (Equation set 50, Briegleb and Light, 2007), where the name "delta" implies CICE implements the Delta-transform to account for the strong forward scattering of snow and sea ice (Equations 2 (a)-(c), Wiscombe and Warren, 1980). The direct albedo and transmittance are computed by equations:

$$R(\mu_{0,n}) = A_n\, exp\left(\frac{-\tau}{\mu_{0,n}}\right) + B_n(exp(\varepsilon_n\tau) - exp(-\varepsilon_n\tau)) - K_n \tag{4a}$$

$$T(\mu_{0,n}) = E_n + H_n(exp(\varepsilon_n\tau) - exp(-\varepsilon_n\tau))\, exp\left(\frac{-\tau}{\mu_{0,n}}\right) \tag{4b}$$

where coefficients A_n, B_n, K_n, E_n, H_n, and ε_n are determined by the single-scattering albedo (ϖ), asymmetry factor (g), optical depth (τ), and angle of incident beam at layer n ($\mu_{0,n}$). Following the delta-Eddington assumption, simple formulas are available for the

The Cryosphere Discuss., https://doi.org/10.5194/tc-2019-22
Manuscript under review for journal The Cryosphere
Discussion started: 20 February 2019

single-layer reflectance and transmittance under both clear sky (direct flux, equations 4a and 4b) and overcast sky (diffuse flux) conditions, however, the formula derived by applying diffuse-flux upper boundary conditions sometimes yields negative albedos (Wiscombe 1977). To avoid the unphysical values, diffuse reflectance $\bar{R}$ and transmittance $\bar{T}$ of a single layer are computed by integrating the direct reflectance $R(\mu)$ and transmittance $T(\mu)$ over the incident hemisphere assuming isotropic incidence:

$$\bar{R} = 2\int_0^1 \mu R(\mu) d\,\mu \tag{5a}$$

$$\bar{T} = 2\int_0^1 \mu T(\mu) d\,\mu \tag{5b}$$

This is the same as the method proposed by Wiscombe and Warren (1980, their equation 5). In practice, eight Gaussian angles are implemented to perform the integration for every layer.

These layer reflectance and transmittance of direct and diffuse components are then combined to account for the inter-layer scattering of light to compute the reflectance and transmission at every interface (Equation set 51, Briegleb and Light, 2007), and eventually the upward and downward fluxes (Equation set 52, Briegleb and Light, 2007). These upward and downward fluxes at each optical depth are then used to compute the column reflectance and transmittance, and the absorption profiles for any multilayered media, such as snowpacks on land and sea ice.

In nature, a large fraction of sea ice is covered by snow during winter. As snow melts away in late spring and summer, it exposes bare ice, and melt ponds form on the ice surface. Such variation of sea-ice surface types requires the shortwave radiative transfer model to be flexible and capable of capturing the light refraction and reflection. Refractive boundaries exist where air (refractive index m_{re} = 1.0), snow (assuming snow as medium of air containing a collection of ice particles, m_{re} = 1.0), pond (assuming pure water, m_{re} = 1.33), and ice (assuming pure ice, m_{re} = 1.31) are present in the same sea-ice column. The general solution of delta-Eddington, and the 2-stream algorithms used in SNICAR are not applicable to such non-uniformly refractive layered media. To include the effects of refraction, Briegleb and Light (2007) modified the adding formula at the refractive boundaries (i.e. interfaces between air/ice, snow/ice, air/pond). The reflectance and transmittance of the adjacent layers above and below the refractive boundary are combined with modifications to include the Fresnel reflection and refraction of direct and diffuse fluxes (Section 4.1, Briegleb and Light, 2007). This adding-doubling delta-Eddington method can thus be applied to any layered media with either uniform (e.g., snow on land) or non-uniform (e.g., snow on sea ice) refractive indexes.

In this paper, we focus on snowpacks that can be treated as uniform refractive media such as the air/snowpack/land columns assumed in SNICAR. An ideal radiative treatment for snow should however keep the potential to include refraction for further applications to snow on sea ice or ice sheets. Therefore, besides these two widely used algorithms in Icepack and SNICAR, we evaluate a third algorithm (section 2.3) that can be applied to layered media with either uniform or non-uniform refractive indexes.

2.3. 2-stream discrete-ordinate algorithm (2SD)

A refractive boundary also exists between the atmosphere and the ocean, and models have been developed to solve the radiative transfer problems in the atmosphere-ocean system using the discrete-ordinate technique (e.g. Jin and Stamnes, 1994; Lee and Liou, 2007). Similar to the 2-stream algorithms of Toon et al., (1989) used in SNICAR, Jin and Stamnes (1994) also developed their algorithm from the general equation:

$$\mu \frac{\partial I}{\partial \tau}(\tau,\mu) = I(\tau,\mu) - \frac{\varpi}{4\pi}\int_{-1}^{1} P(\tau,\mu,\mu')\, I(\tau,\mu') d\mu' - S(\tau,\mu) \tag{6}$$

Equation (6) is the azimuthally integrated version of equation (1). However, for vertically inhomogeneous media like the atmosphere-ocean or sea ice, the external source term $S(\tau,\mu)$ is different. Specifically, for the medium of total optical depth τ^a above the refractive interface, one must consider the contribution from the upward beam reflected at the refractive boundary (second term on the right-hand side):

$$S^a(\tau,\mu) = \frac{\varpi}{4\pi} F_s P(\tau,-\mu_0,\mu)\, exp\left(\frac{-\tau}{\mu_0}\right) + \frac{\varpi}{4\pi} F_s R(-\mu_0,m) P(\tau,+\mu_0,\mu) exp\left(\frac{-(2\tau^a-\tau)}{\mu_0}\right) \tag{7}$$

where $R(-\mu_0,m)$ is the Fresnel reflectance of radiation and m is the ratio of the refractive indices of the lower to the upper medium. For the medium below the refractive interface, one must account for the Fresnel transmittance $T(-\mu_0,m)$ and modify the angle of beam travel in media b:

The Cryosphere Discuss., https://doi.org/10.5194/tc-2019-22
Manuscript under review for journal The Cryosphere
Discussion started: 20 February 2019

$$S^b(\tau,\mu) = \frac{\varpi}{4\pi}\frac{\mu_0}{\mu_{0n}} F_s T(-\mu_0, m) P(\tau, -\mu_0, \mu)\, exp\left(\frac{-\tau^a}{\mu_0}\right) exp\left(\frac{-(\tau-\tau^a)}{\mu_{0n}}\right) \quad (8)$$

where μ_{0n} is the cosine zenith angle of refracted beam incident at angle μ_0 above refractive boundary, by Snell's law:

$$\mu_{0n} = \sqrt{1-(1-\mu_0^2)/m^2} \quad (9)$$

For uniformly refractive media like snow on land, one can just set the refractive index m_{re} equal to 1 for every layer. In this case, the Fresnel reflectance $R(-\mu_0, m)$ is 0 in equation (7), the Fresenal transmittance $T(-\mu_0, m)$ is 1 in equation (8), and μ_{0n} equals to μ_0: the two source terms $S^a(\tau,\mu)$ and $S^b(\tau,\mu)$ become the same and equal to the source term of homogenous media given in equation (2).

For 2-stream approximations of this method, analytical solutions of upward and downward fluxes are coupled at each layer interface to generate 2N equations with 2N unknown coefficients for any N-layer stratified column. The solutions of 2-stream algorithms and boundary conditions for homogenous media are well documented (Sections 8.4 and 8.10 of Thomas and Stamnes, 1999). Despite the extra source terms, these 2N equations can also be organized into a tridiagonal matrix similar to the method of Toon et al. (1989) used in SNICAR. Flexibility and speed therefore make this 2-stream discrete-ordinate algorithm (hereafter, 2SD) a potentially good candidate for long-term Earth system modeling. In this work, we only apply 2SD to snowpack and note that it can be applied to any uniformly or non-uniformly refractive media like snow on land or sea ice, with the Delta-transform implemented to fundamental optical variables (Equations 2 (a)-(c), Wiscombe and Warren, 1980).

2.4 16-stream DISORT

Besides the mathematical technique, the accuracy and speed of radiative transfer algorithms depend on the number of angles used for flux estimation in the upward and downward hemispheres. The algorithms used in SNICAR, Icepack, and 2SD use one angle to represent upward flux and one angle to represent downward flux, hence they are named 2-stream algorithm. Lee and Liou (2007) use two upward and two downward streams. Jin and Stamnes (1994) documented the solutions for any even number of streams. The speed of these models is slower than 2-stream models while their accuracy is better. To quantify the accuracy of the three 2-stream algorithms for snow shortwave simulations, we use the 16-stream DIScrete-Odinate Radiative Transfer model (DISORT) as the benchmark model (http://lllab.phy.stevens.edu/disort/) (Stamnes et al., 1988).

3. Input for radiative transfer models

In this work, we focus on the performance of 2-stream algorithms for pure snow simulations. The inputs for these three models are the same: single-scattering properties (SSPs, i.e. single-scattering albedo ϖ, asymmetry factor g, extinction coefficient σ_{ext}) of snow determined by snow grain radius r, snow depth, solar zenith angle θ, solar incident flux, and the albedo of underlying ground (assuming Lambertian reflectance of 0.25 for all wavelengths). A Delta-transform is applied to fundamental input optical variables for all simulations (Equations 2 (a)-(c), Wiscombe and Warren, 1980).

In snow, photon scattering occurs at the air-ice interface, and the absorption of photons occurs within the ice crystal. The most important factor that determines snow shortwave properties is the ratio of total surface area to total mass of snow grains, aka "the specific surface area" (e.g. Matzl and Schneebeli, 2006, 2010). The specific surface area (β) can be converted to a radiatively effective snow grain radius r:

$$\beta = 3 / (r\,\rho_{ice}) \tag{10}$$

where ρ_{ice} is the density of pure ice, 917 kg m^{-3}. Assuming the grains are spherical, the SSPs of snow can thus be computed using Mie theory (Wiscombe, 1980) and ice optical constants (Warren and Brandt, 2008). In nature, snow grains are not spherical, and many studies have been carried out to quantify the accuracy of such spherical representations (Grenfell and Warren, 1999; Neshyba et al., 2003; Grenfell et al., 2005). In recent years, more research has been done to evaluate the impact of grain shape on snow shortwave properties (Dang et al., 2016; He et al., 2017, 2018ab), and they show that non-spherical snow grain shapes mainly alter the asymmetry factor. Dang et al., (2016) also point out that the solar properties of a snowpack consisting of non-spherical ice grains can be mimicked by a snowpack consisting of spherical grains with a smaller grain size by factors up to 2.4. In this work, we still assume the snow grains are spherical, and this assumption does not qualitatively alter our evaluation of the radiative transfer algorithms.

The Cryosphere Discuss., https://doi.org/10.5194/tc-2019-22
Manuscript under review for journal The Cryosphere
Discussion started: 20 February 2019

The input SSPs of snow grains are computed using Mie theory at fine spectral resolution for a wide range of ice effective radius *r* from 10 to 3000 µm that covers the possible range of grain radius for snow on Earth (Flanner et al., 2007). The same spectral SSPs were also used to derive the band-averaged SSPs of snow used in SNICAR. Note Briegleb and Light (2007) refer to SSPs as inherent optical properties.

4. Solar spectra used for the spectral integrations

In climate modeling, snow albedo computation at fine spectral resolution is expensive and unnecessary. Instead of computing spectrally resolved snow albedo as shown in Figure 1, wider-band solar properties are more practical. For example, CESM and E3SM aggregate the narrow RRTMG bands used for the atmospheric radiative transfer simulation into visible (0.2 - 0.7 µm) and near-IR (0.7 - 5 µm) bands. The land model and sea-ice model thus receive visible and near-IR fluxes as the upper boundary condition, and return the corresponding visible and near-IR albedos to atmosphere model. In practice, these bands are also partitioned into direct and diffuse components. Therefore, a practical 2-stream algorithm should be able to simulate the direct visible, diffuse visible, direct near-IR and diffuse near-IR albedos and absorptions of snow accurately.

The band albedo α is an irradiance-weighted average of the spectral albedo $\alpha(\lambda)$:

$$\alpha = \frac{\int_{\lambda 1}^{\lambda 2} \alpha(\lambda) F(\lambda) d\lambda}{\int_{\lambda 1}^{\lambda 2} F(\lambda) d\lambda} \tag{11}$$

In this work, we use the spectral irradiance $F(\lambda)$ generated by the atmospheric DISORT-based Shortwave Narrowband Model (SWNB2) (Zender et al., 1997; Zender, 1999) for typical clear-sky and cloudy-sky conditions of mid-latitude winter as shown in Figure 1(a). The total clear-sky down-welling surface flux at different solar zenith angles are also given in Figure 1(b).

5. Model Evaluation

5.1 Spectral albedo and reflected solar flux

The spectral reflectance of pure deep snow computed using 2-stream models and 16-stream DISORT are shown in Figure 2. The snow grain radius is 100 µm - a typical grain size for fresh new snow. For clear sky with direct beam source (left column), all three 2-stream models show good accuracy at visible wavelengths (0.3 – 0.7 µm), and within this band, the snow albedo is large and close to 1. As wavelength increases, the albedo diminishes in the near-IR band. 2-stream models overestimate snow albedo at these wavelengths, with maximum biases of 0.013 (SNICAR and CICE) and 0.023 (2SD) within wavelength 1 - 1.7 μm. For cloudy-sky cases with diffuse upper boundary conditions, CICE reproduces the snow albedo at all wavelengths with the smallest absolute error (< 0.005), SNICAR and 2SD both overestimate the snow albedo with maximum biases > 0.04 between 1.1-1.4 μm.

In both sky conditions, the errors of snow albedo are larger at near-IR wavelengths ranging from 1.0-1.7 μm, while the solar incident flux peaks at 0.5 μm then decreases as wavelength increases. The largest error in reflected flux is within the 0.7-1.5 μm band for SNICAR and 2SD, as shown in the 3rd row of Figure 2. CICE overestimate the direct snow albedo mostly at wavelengths larger than 1.5 μm where the error in reflected flux is almost negligible.

5.2 Broadband albedo and reflected solar flux

Integrated over the visible and near-IR wavelengths, the error in band albedos computed using 2-stream models for different cases are shown in Figure 3-6.

Figure 3 shows the error in direct band albedo for fixed snow grain radius of 100 μm with different snow depth and solar zenith angles. As introduced in Section 2, SNICAR and CICE both use delta-Eddington method to compute the visible albedo. They overestimate the visible albedo for solar zenith angles smaller than 50° by up to 0.005, and underestimate it for solar zenith angles larger than 50° by up to -0.01. 2SD produces similar results for the visible band but at a larger solar zenith angle threshold of 75°. In the near-IR band, SNICAR and 2SD overestimate the snow albedo for solar zenith angles smaller than 70°, beyond this, the error in albedo increases by up to -0.1 as solar zenith angle increases. CICE produces a similar error pattern with a smaller solar zenith angle threshold at 60°. As snow ages, its average grain size increases. For typical old melting snow of grain radius 1000 μm (Figure 4), 2-stream models produce similar errors of direct albedo in all bands. For snow consisting of smaller grain size, 2-stream models produce larger errors for visible albedo. Integrating over the entire solar band, the three 2-stream models evaluated show similar error patterns for direct albedo.

For a fixed solar zenith angle of 60°, the error of direct albedo for different snow depth and snow grain radii are shown in Figure 5. SNICAR and CICE underestimate the visible albedo in most scenarios, while 2SD overestimates the visible albedo for a larger range of grain radius and snow depth. All three 2-stream models tend to overestimate the near-IR albedo except for shallow snow with large grain radius; the error of 2SD is one order of magnitude larger than that of SNICAR and CICE.

Figure 6 is similar to Figure 5, but shows the diffuse snow albedo. In the visible band, SNICAR and CICE generate similar errors in that they both underestimate the albedo as snow grain size increases and snow depth decreases. 2SD overestimates the albedo with maximum error of around 0.015. In the near-IR, 2-stream models tend to overestimate snow albedo, while the magnitude of biases produced by SNICAR and 2SD are one order larger than that of CICE with the maximum error of 0.035 generated by SNICAR. As a result, the all-wave diffuse albedos computed using CICE are more accurate than those computed using SNICAR and 2SD.

Figures 7, 8 and 9 show the errors in reflected shortwave flux caused by snow albedo errors seen in Figures 3, 4, and 6. In general, 2-stream models produce larger errors in reflected direct near-IR flux (Figure 7 and 8), especially with the 2SD model: the maximum overestimate of reflected near-IR flux is 6-8 Wm^{-2} for deep melting snow with solar zenith angle < 30°. Errors in reflected direct visible flux are smaller (mostly within ±1 Wm^{-2}) for all models in most scenarios, and become larger (mostly within ±3 Wm^{-2}) as snow grain size increases to 1000 μm if computed using 2SD. As shown in Figure 9, for diffuse flux with solar zenith angle of 60° at TOA, SNICAR and CICE generate small errors in reflected visible flux (mostly within ±1 Wm^{-2}), while 2SD always overestimates reflected visible flux by up to 5 Wm^{-2}. In the near-IR, SNICAR and 2SD overestimate reflected flux by as much as 10-12 Wm^{-2}; the error in reflected near-IR flux produced by CICE is much smaller, mostly within ±1 Wm^{-2}.

In general, CICE produces the most accurate albedo and thus reflected flux for both direct and diffuse components. SNICAR is similar to CICE for its accuracy of direct albedo and flux, yet generates large error for diffuse component. 2SD tends to overestimate snow albedo and reflected flux in both direct and diffuse components and shows the largest errors among three 2-stream models. Note that the final errors of snow albedo and reflected solar flux are the weighted sum of direct and diffuse components, and their weights are largely determined by cloud cover fraction (e.g. Figure 6, Dang et al., 2017), which we do not address explicitly in this paper.

The Cryosphere Discuss., https://doi.org/10.5194/tc-2019-22
Manuscript under review for journal The Cryosphere
Discussion started: 20 February 2019

5.3 Band absorption of solar flux

Figure 10 shows absorption profiles of shortwave flux computed using the 16-stream DISORT model, with errors in absorbed fractional solar flux computed using 2-stream models. The snowpack is 10-cm deep, and is divided into 5 layers, each 2-cm thick. The snow grain radius is set to 100 µm. The figure shows fractional absorption for snow layers 1-4 and the underlying ground with albedo of 0.25.

As shown in the first column of Figure 10, for new snow with radius of 100 µm, most solar absorption occurs in the top 2-cm snow layer, where roughly 10% and 15% of diffuse and direct near-IR flux are absorbed and dominate the solar absorption within snowpack. In the second layer (2-4 cm), the absorption of solar flux is less than 1% and gradually decreases within the interior layers. The underlying ground absorbs roughly 2% of solar flux, mostly visible flux that penetrates the snowpack more efficiently. As snow ages and snow grain grows, photons penetrate deeper into the snowpack. For typical old melting snow with radius of 1000 µm, most solar absorption still occurs in the top 2-cm snow layer, where roughly 20% and 14% of diffuse and direct near-IR flux are absorbed. The second snow layer (2-4 cm) absorbs more near-IR solar flux by roughly 2%. More photons are able to penetrate through the snowpack, and results in a high fractionally absorption by the underlying ground, especially for visible band. As snow depth increase, the ground absorption will decrease for both snow radii.

Comparing to 16-stream DISORT, 2-stream models underestimate (overestimate) the column solar absorptions for new (old) snow, especially for the surface snow layer and ground layer. Overall, CICE gives the most accurate absorption profiles among three 2-stream models, especially for new snow.

6. Correction for direct albedo for large solar zenith angles

It has been pointed out in previous studies that the 2-stream approximations become poor as solar zenith angle approaches 90° (e.g. Wiscombe 1997, Warren 1982). As shown in Figures 3 and 4, all three 2-stream models underestimate the direct snow albedo for large solar zenith angles. In the visible band, when snow grain size is small, the error in direct albedo is almost negligible (Figure 3); while as snow ages and snow grains become larger, the error increases yet still remains low if the snow is deep (Figure 4). In the near-IR, the biases of albedo are also larger for larger snow grain radii. For a given snow size,

The Cryosphere Discuss., https://doi.org/10.5194/tc-2019-22
Manuscript under review for journal The Cryosphere
Discussion started: 20 February 2019

the magnitudes of such biases are almost independent of snow depth, and mainly determined by the solar zenith angle. In general, the errors of all-wave direct albedo are mostly contributed by the errors of near-IR albedo, especially for optically thick snowpacks (i.e., semi-infinite), because the errors of direct albedo in the visible are negligible compared with those in the near-IR. To improve the performance of 2-stream algorithms, we develop a parameterization that corrects the underestimated near-IR snow albedo at large zenith angles.

Figure 11 shows the direct near-IR albedo and fractional absorption of a 2-meter thick snowpacks consisting of grains with radius 100 μm and 1000 μm, computed using 2-stream algorithms and 16-stream DISORT. For solar zenith angles > 75°, 2-stream models underestimate snow albedo and overestimate solar absorption within snowpack, mostly in the top 2-cm of snow. We define and compute R_{75+} as the ratio of direct semi-infinite near-IR albedo computed using 16-stream DISORT ($\alpha_{16\text{-}DISORT}$) to that computed using CICE (α_{CICE}). This ratio is shown in Figure 11 (c) and can be parameterized as a function of snow grain radius (r, unit in meter) and the cosine of incident solar zenith angle (μ_0), as shown in Figure 11(c):

$$R_{75+} = \frac{\alpha_{16-DISORT}}{\alpha_{CICE}} = c_1(\mu_0)log_{10}(r) + c_0(\mu_0) \quad (12)$$

where coefficients c_1 and c_0 are polynomial functions of μ_0, as shown in Figure 11(d):

$$c_1(\mu_0) = 1.304\mu_0^2 - 0.631\mu_0 + 0.086 \quad (13a)$$

$$c_0(\mu_0) = 6.807\mu_0^2 - 3.338\mu_0 + 1.467 \quad (13b)$$

Since 2-stream models always underestimate snow albedo, R_{75+} always exceeds 1 (Figure 11c). We can then adjust the direct near-IR snow albedo (α_{CICE}) and direct near-IR solar absorption ($Fabs_{CICE}$) by snow computed using CICE with ratio R_{75+}:

$$\alpha_{CICE}^{adjust} = R_{75+}\alpha_{CICE} \quad (14a)$$

$$Fabs_{CICE}^{adjust} = Fabs_{CICE} - (R_{75+} - 1) * \alpha_{CICE} * F_{nir} \quad (14b)$$

where F_{nir} is the direct near-IR flux. This adjustment reduces the error of near-IR albedo from negative 2-10% to within ± 0.5% for solar zenith angles larger than 75°, and for grain radii ranging from 30-1500 μm (Figure 12). Errors in broadband direct albedo are therefore also reduced to < 0.01. The direct near-IR flux absorbed by the snowpack decreases after applying this adjustment. In practice, if snow is divided into multiple layers, we assume all decreased near-IR absorption (2nd term on the right hand side, equation 14b) is confined within the top layer. This assumption is fairly accurate for the near-IR band, since most direct IR absorption occurs at the very surface of snowpack (Figures 10 and 11).

It is important to note that although the errors of direct near-IR albedos are large for large solar zenith angles, the absolute error in reflected shortwave flux is small (Figures 7 and 8) as the down-welling solar flux reaches snowpack decreases as solar zenith angle increases (Figures 1(b)). However, such small biases in flux can be important at high latitudes where the solar zenith angle remains large for many days in late winter and early spring. We have implemented this parameterization in MPAS-seaice to quantify its impact on polar climate, though these experiments are beyond the scope of the present paper.

7. Implementation of snow radiative transfer model in Earth system models

ESMs often use broader band-averaged SSPs of snow and aerosols for computational efficiency, rather than using brute-force integration of spectral solar properties across narrower bands (per equation 11). Besides using different radiative transfer approximations, SNICAR and CICE also adopt different methods to derive the band-averaged SSPs of snow for different band schemes.

In SNICAR, snow solar properties are computed for 5 bands: one visible band (0.3 - 0.7μm), and four near-IR bands (0.7 - 1 μm, 1 – 1.2 μm, 1.2 – 1.5 μm, and 1.5 – 5 μm). The solar properties of four subdivided near-IR bands are combined by fixed ratios to compute the direct/diffuse near-IR snow properties. These two sets of ratios are derived offline based on the incident solar spectra of typical of mid-latitude winter for clear and cloudy-sky conditions clear sky and cloudy sky, respectively (Figure 1(a)).

The band-averaged SSPs of snow grains are computed following the Chandrasekhar Mean approach (Thomas and Stamnes, 1999, their Equation 9.27; Flanner et al., 2007).

The Cryosphere Discuss., https://doi.org/10.5194/tc-2019-22
Manuscript under review for journal The Cryosphere
Discussion started: 20 February 2019

Specifically, spectral SSPs of snow grains are weighted into bands according to surface incident solar flux typical of mid-latitude winter for clear and cloudy sky conditions. In addition, the single-scattering albedo $\varpi(\lambda)$ of ice grains are also weighted by the hemispheric albedo $\alpha(\lambda)$ of an optically thick snowpack:

$$\varpi(\bar{\lambda}) = \frac{\int_{\lambda_1}^{\lambda_2} \varpi(\lambda)F(\lambda)\alpha(\lambda)d\lambda}{\int_{\lambda_1}^{\lambda_2} F(\lambda)\alpha(\lambda)d\lambda} \quad (15a)$$

$$g(\bar{\lambda}) = \frac{\int_{\lambda_1}^{\lambda_2} g(\lambda)F(\lambda)d\lambda}{\int_{\lambda_1}^{\lambda_2} F(\lambda)\alpha(\lambda)d\lambda} \quad (15b)$$

$$\sigma_{ext}(\bar{\lambda}) = \frac{\int_{\lambda_1}^{\lambda_2} \sigma_{ext}(\lambda)F(\lambda)d\lambda}{\int_{\lambda_1}^{\lambda_2} F(\lambda)\alpha(\lambda)d\lambda} \quad (15c)$$

Two sets of snow band-averaged SSPs are generated for all grain radii, suitable for direct and diffuse light, respectively. For each modeling step and band, SNICAR is called twice to compute the direct and diffuse snow solar properties.

In CICE, the snow-covered sea ice properties are computed for 3 bands: one visible band (0.3 – 07 μm), and two near-IR bands (0.7 – 1.19 μm and 1.19 – 5 μm). The solar proprieties of these two near-IR bands are combined using ratios w_{nir1} and w_{nir2} for 0.7-1 .19 μm and 1.19-5 μm, depending on the fraction of direct near-IR flux f_{nidr}:

$$w_{nir1} = 0.67 + 0.11 * (1 - f_{nidr}) \quad (16a)$$

$$w_{nir2} = 1 - w_{nir1} \quad (16b)$$

The band SSPs of snow are derived by integrating the spectral SSPs and the spectral surface solar irradiance measured in the Arctic under mostly clear sky.

$$\varpi(\bar{\lambda}) = \int_{\lambda_1}^{\lambda_2} \varpi(\lambda)F(\lambda)d\lambda \quad (17a)$$

$$g(\bar{\lambda}) = \int_{\lambda_1}^{\lambda_2} g(\lambda)F(\lambda)d\lambda \quad (17b)$$

$$\sigma_{ext}(\bar{\lambda}) = \int_{\lambda_1}^{\lambda_2} \sigma_{ext}(\lambda)F(\lambda)d\lambda \quad (17c)$$

The Cryosphere Discuss., https://doi.org/10.5194/tc-2019-22
Manuscript under review for journal The Cryosphere
Discussion started: 20 February 2019

In addition, the band-averaged single-scattering albedo $\varpi(\bar{\lambda})$ is also increased to $\varpi(\bar{\lambda})'$ until the band albedo computed using averaged SSPs matches the band albedo $\bar{\alpha}$ within 0.0001, where $\bar{\alpha}$ is:

$$\bar{\alpha} = \int_{\lambda_1}^{\lambda_2} \alpha(\lambda)F(\lambda)d\lambda \quad (18)$$

CICE adopts this single set of band SSPs for both direct and diffuse computations. In practice, the physical snow grain radius r is adjusted to a radiatively equivalent radius r_{eqv} based on the fraction of direct flux in the near-IR band (f_{nidr}):

$$r_{eqv} = (f_{nidr} + 0.8(1 - f_{nidr}))r \quad (19)$$

This r_{eqv} and the corresponding snow SSPs are then used in the radiative transfer calculation. The computed direct and diffuse solar properties alone are less accurate, while the combined all-sky broadband solar properties agree with SNICAR (Briegleb and Light, 2007). As a result, for each modeling step and band, CICE radiative transfer subroutine is called only once to compute both the direct and diffuse snow solar properties simultaneously.

SNICAR and CICE also use different approaches to avoid numerical singularities. In SNICAR, singularities occur when the denominator of term $C_n^{\pm}$ in equation (3) equals to zero (i.e., $\gamma^2 - 1/\mu_0^2 = 0$), where γ is determined by the approximation method and SSPs of snow, and μ_0 is the cosine of the solar zenith angle (Equations 23 and 24, Toon et al., 1989). When such a singularity is detected, SNICAR will shift μ_0 by + 0.02 or -0.02 to obtain physically realistic radiative properties. In the CICE algorithm, singularities arise only when $\mu_0 = 0$ (Equation 4). Therefore, in practice, for $\mu_0 < 0.01$, CICE computes the sea-ice solar properties for $\mu_0 = 0.01$ to avoid unphysical results.

8. Discussion: a unified radiative transfer model for snow, sea ice, and land ice.

Based on the inter-comparison of three 2-stream algorithms and their implementations in ESMs, we formulated the following surface shortwave radiative transfer

The Cryosphere Discuss., https://doi.org/10.5194/tc-2019-22
Manuscript under review for journal The Cryosphere
Discussion started: 20 February 2019

recommendations for an accurate, fast, and consistent treatment for snow on land, land ice, and sea ice in ESMs:

First, the 2-stream delta-Eddington adding-doubling algorithm by Briegleb and Light (2007) is unsurpassed as a radiative transfer core. The evaluation in Section 5 shows that this algorithm produces the least error for snow albedo and solar absorption within snowpack, especially under overcast sky. This algorithm applies well to both uniformly refractive media such as snow on land, and to non-uniformly refractive media, such as bare/snow-covered/ponded sea ice and bare/snow-covered land ice. Numerical singularities occur only rarely (when $\mu_0 = 0$) and are easily avoided in model implementations. Among the three 2-stream algorithms discussed here, the CICE radiative core is also the most efficient one as it takes only ~2/3 of the time of SNICAR and 2SD to compute solar properties of multi-layer snowpacks.

Second, any 2-stream cryospheric radiative transfer model can incorporate the parameterization described in Section 6 to adjust the low bias of direct near-IR snow albedo and high bias of direct near-IR solar absorption in snow, for solar zenith angles larger than 75°. These biases are persistent across all 2-stream algorithms discussed in this work, and should be corrected for snow-covered surfaces. Alternatively, adopting a 4-stream approximation would reduce or eliminate such biases, though at considerable expense in computational efficiency.

Third, a cryospheric radiative transfer model should prefer physically based parameterizations that are extensible and convergent (e.g., with increasing spectral resolution) for the band-averaged SSPs and size distribution of snow. Although the treatments used in SNICAR and CICE are both practical since they both reproduce the narrowband solar properties with carefully derived band-averaged inputs as discussed in Section 7, the snow treatment used in SNICAR is more physically based and reproducible since it does not rely on subjective adjustment and empirical coefficients as used in CICE. Specifically, the empirical adjustment to snow grain radius implemented in CICE may not always produce compensating errors. For example, in snow containing light-absorbing impurities such adjustment may also lead to biases in aerosol absorption since the albedo reduction caused by light-absorbing particles does not linearly depend on snow grain radius (Dang et al., 2015). For further model development incorporating non-spherical snow grain shapes (Dang et al., 2016; He et al., 2018ab), such adjustment on grain radius may fail as well. Moreover, SNICAR computes the snow properties for four near-IR bands, which helps capture the spectral variation of albedo (Figure 2) and therefore better represents near-IR solar properties. It is also worth noting that unlike the radiative core of CICE, SNICAR is actively maintained with numerous modifications and updates in the past decade (e.g. Flanner et al., 2012; He et al., 2018b). Snow radiative treatments that follow SNICAR conventions for SSPs may take advantage of these updates. Note that any radiative core that follows SNICAR SSP conventions must be called twice to compute diffuse and direct solar properties, respectively.

Fourth, a surface cryospheric radiative transfer model should flexibly accommodate coupled simulations with distinct atmospheric and surface spectral grids. Both the 5-band scheme used in SNICAR and the 3-band scheme used in CICE separate the visible from near-IR spectrum at 0.7 μm. This boundary aligns with the Community Atmospheric Model's original radiation bands (CAM; Neale et al., 2012), though not with the widely used Rapid Radiative Transfer Model (RRTMG; Iacono et al., 2008) which places 0.7 μm squarely in the middle of a spectral band. A mismatch in spectral boundaries between atmospheric and surface radiative transfer schemes can require an ESM to unphysically apportion energy from the straddled spectral bin when coupling fluxes between surface and atmosphere. The spectral grids of surface and atmosphere radiation need not be identical so long as the coarser grid shares spectral boundaries with the finer grid. In practice maintaining a portable cryospheric radiative module such as SNICAR requires a complex offline toolchain (Mie solver, spectral refractive indices for air, water, ice, and aerosols, spectral solar insolation for clear and cloudy skies) to compute, integrate, and rebin SSPs. Aligned spectral boundaries between surface and atmospheric would simplify the development of efficient and accurate radiative transfer for the coupled Earth system.

Last, it is important to note that, although we only examine the performance of the CICE adding-doubling algorithm for pure snow in this work, this algorithm can be applied to the surface solar calculation of all cryospheric components with or without light-absorbing particles present. First, Briegleb and Light (2007) proved its accuracy for simulating ponded/bare sea-ice solar properties against observations and a Monte Carlo radiation model. Second, In CESM and E3SM, the radiative transfer simulation of snow on land ice is carried out by SNICAR with prescribed land ice albedo. Adopting the CICE adding-doubling core in SNICAR will permit these ESMs to couple the snow and land ice as a non-uniformly refractive column for more accurate solar computations since bare/snow-covered/ponded land ice is physically similar to bare/snow-covered/ponded sea ice, and the latter is already treated well by CICE radiative transfer core. Third, adding light-absorbing particles in snow will not change our results qualitatively. Both CICE and SNICAR simulate the impact of light-absorbing particles (black carbon and dust) on snow and/or sea ice using self-consistent particle SSPs that follow the SNICAR convention. The adoption of CICE radiative transfer algorithm in SNICAR, and the implementation of SNICAR snow SSPs in CICE will enable a consistent simulation on the radiative effects of light-absorbing particles in the cryosphere across ESM components.

In summary, this inter-comparison and evaluation has shown multiple ways that the solar properties of cryospheric surfaces can be improved in the current generation of ESMs. We have adopted these recommendations in a hybrid model SNICAR-AD, implemented in MPAS-seaice and E3SM Land Model (ELM), to examine the response of climate to this improved and unified cryospheric surface radiation treatment in future E3SM studies.

9. Conclusions

In this work, we aim to improve and unify the solar radiative transfer calculations for snow on land and snow on sea ice in ESMs by evaluating the following 2-stream radiative transfer algorithms: the 2-stream delta-Eddington adding-doubling algorithm implemented in sea-ice model Icepack/CICE/MPAS-seaice, the 2-stream delta-Eddington and 2-stream delta-Hemispheric-Mean algorithms implemented in snow model SNICAR, and a 2-stream delta-Discrete-Ordinate algorithm. Among these three models, the 2-stream delta-Eddington adding-doubling algorithm produces the most accurate snow albedo and solar absorption (Section 5). All 2-stream models underestimate near-IR snow albedo and overestimate near-IR absorption when solar zenith angles are larger than 75°, which can be adjusted by a parameterization we developed (Section 6). We compared the implementations of radiative transfer cores in SNICAR and CICE (Section 7) and recommended a consistent shortwave radiative treatment for snow-covered surfaces across ESMs (Section 8). Improved treatment of surface cryospheric radiative properties in the thermal infrared has recently been shown to remediate significant climate simulation biases in Polar Regions (Huang et al., 2018). It is hoped that adoption of improved and consistent treatments of solar radiative properties for snow-covered surfaces as described in this study (i.e. the hybrid model SNICAR-AD) will further remediate simulation biases in Polar Regions.

Data availability. The data and models are available upon request to Cheng Dang (cdang5@uci.edu). SNICAR and CICE radiative transfer core can be found at https://github.com/E3SM-Project/E3SM.

Competing interests. The authors declare that they have no conflict of interest.

Acknowledgements. The authors thank Prof. Stephen G. Warren and Prof. Qiang Fu for helpful discussions on radiative transfer algorithms. The authors thank Dr. Adrian Turner for instructions on installing and running MPAS-seaice. This research was supported as part of the Energy Exascale Earth System Model (E3SM) project, funded by the U.S. Department of Energy, Office of Science, Office of Biological and Environmental Research, with funding number DOE BER ESM (DE-SC0012998).

References

Aoki, T., Kuchiki, K., Niwano, M., Kodama, Y., Hosaka, M. and Tanaka, T.: Physically based snow albedo model for calculating broadband albedos and the solar heating profile in snowpack for general circulation models. Journal of Geophysical Research, 116, D11114, https://doi.org/10.1029/2010JD015507, 2011.

Bøggild, C.E., Brandt, R.E., Brown, K.J. and Warren, S.G.: The ablation zone in northeast Greenland: ice types, albedos and impurities. Journal of Glaciology, 56, 101-113, pp.101-113, https://doi.org/10.3189/002214310791190776, 2010.

Brandt, R.E., Warren, S.G., Worby, A.P. and Grenfell, T.C.: Surface albedo of the Antarctic sea ice zone. Journal of Climate, 18(17), pp.3606-3622. https://doi.org/10.1175/JCLI3489.1 2005.

Briegleb, P. and Light, B.: A Delta-Eddington mutiple scattering parameterization for solar radiation in the sea ice component of the community climate system model, 2007.

Dang, C. and Hegg, D.A.: Quantifying light absorption by organic carbon in Western North American snow by serial chemical extractions. Journal of Geophysical Research, 119(17), pp.10-247. https://doi.org/10.1002/2014JD022156, 2014.

Dang, C., Fu, Q. and Warren, S.G., 2016. Effect of snow grain shape on snow albedo. Journal of the Atmospheric Sciences, 73(9), pp.3573-3583. https://doi.org/10.1175/JAS-D-15-0276.1, 2016.

Dang, C., Brandt, R.E. and Warren, S.G.: Parameterizations for narrowband and broadband albedo of pure snow and snow containing mineral dust and black carbon. Journal of Geophysical Research: Atmospheres, 120(11), pp.5446-5468, https://doi.org/10.1002/2014JD022646, 2015.

Dang, C., Warren, S.G., Fu, Q., Doherty, S.J., Sturm, M. and Su, J.: Measurements of light-absorbing particles in snow across the Arctic, North America, and China:

Effects on surface albedo. Journal of Geophysical Research: Atmospheres, 122(19), pp.10-149. https://doi.org/10.1002/2017JD027070, 2017.

Doherty, S.J., Hegg, D.A., Johnson, J.E., Quinn, P.K., Schwarz, J.P., Dang, C. and Warren, S.G.: Causes of variability in light absorption by particles in snow at sites in Idaho and Utah. Journal of Geophysical Research: Atmospheres, 121(9), pp.4751-4768. https://doi.org/10.1002/2015JD024375, 2016.

Doherty, S.J., Warren, S.G., Grenfell, T.C., Clarke, A.D. and Brandt, R.E.: Light-absorbing impurities in Arctic snow. Atmospheric Chemistry and Physics. 10(23), pp.11647-11680. https://doi.org/10.5194/acp-10-11647-2010, 2010.

Doherty, S.J., Dang, C., Hegg, D.A., Zhang, R. and Warren, S.G.: Black carbon and other light-absorbing particles in snow of central North America. Journal of Geophysical Research: Atmospheres, 119(22), pp.12-807, https://doi.org/10.1002/2014JD022350, 2014.

Flanner, M.G. and Zender, C.S.: Snowpack radiative heating: Influence on Tibetan Plateau climate. Geophysical Research Letters, 32(6). https://doi.org/10.1029/2004GL022076, 2005.

Flanner, M.G., Zender, C.S., Randerson, J.T. and Rasch, P.J.: Present-day climate forcing and response from black carbon in snow. Journal of Geophysical Research: Atmospheres, 112(D11). https://doi.org/10.1029/2006JD008003, 2007.

Flanner, M.G., Liu, X., Zhou, C., Penner, J.E. and Jiao, C.: Enhanced solar energy absorption by internally-mixed black carbon in snow grains. Atmospheric Chemistry and Physics, 12(10), pp.4699-4721. https://doi.org/10.5194/acp-12-4699-2012, 2012.

Gardner, A.S. and Sharp, M.J.: A review of snow and ice albedo and the development of a new physically based broadband albedo parameterization. Journal of Geophysical Research: Earth Surface, 115(F1). https://doi.org/10.1029/2009JF001444, 2010.

Grenfell, T.C., Neshyba, S.P. and Warren, S.G.: Representation of a nonspherical ice particle by a collection of independent spheres for scattering and absorption of radiation: 3. Hollow columns and plates. Journal of Geophysical Research: Atmospheres, 110(D17). https://doi.org/10.1029/2005JD005811, 2005.

He, C., Liou, K.N., Takano, Y., Yang, P., Qi, L. and Chen, F.: Impact of grain shape and multiple black carbon internal mixing on snow albedo: Parameterization and radiative effect analysis. Journal of Geophysical Research: Atmospheres, 123(2), pp.1253-1268. https://doi.org/10.1002/2017JD027752, 2018a.

He, C., Flanner, M.G., Chen, F., Barlage, M., Liou, K.N., Kang, S., Ming, J. and Qian, Y.: Black carbon-induced snow albedo reduction over the Tibetan Plateau: uncertainties from snow grain shape and aerosol–snow mixing state based on an updated SNICAR model. Atmospheric Chemistry and Physics, 18, pp.11507-11527. https://doi.org/10.5194/acp-18-11507-2018, 2018b.

He, C., Takano, Y., Liou, K.N., Yang, P., Li, Q. and Chen, F.: Impact of Snow Grain Shape and Black Carbon–Snow Internal Mixing on Snow Optical Properties: Parameterizations for Climate Models. Journal of Climate, 30(24), pp.10019-10036. https://doi.org/10.1175/JCLI-D-17-0300.1, 2017.

The Cryosphere Discuss., https://doi.org/10.5194/tc-2019-22
Manuscript under review for journal The Cryosphere
Discussion started: 20 February 2019

The Cryosphere Discussions
Open Access
EGU

Huang, X., Chen, X., Flanner, M., Yang, P., Feldman, D. and Kuo, C.: Improved representation of surface spectral emissivity in a global climate model and its impact on simulated climate. Journal of Climate, 31(9), pp.3711-3727. https://doi.org/10.1175/JCLI-D-17-0125.1, 2018.

Hunke, E. C., Lipscomb, W. H., Turner, A. K., Jeffery, N., and Elliott, S.: CICE: the Los Alamos Sea Ice Model Documentation and Software User's Manual Version 4.1 LA-CC-06-012. T-3 Fluid Dynamics Group, Los Alamos National Laboratory 675. 2010.

Iacono, M.J., Delamere, J.S., Mlawer, E.J., Shephard, M.W., Clough, S.A. and Collins, W.D.: Radiative forcing by long‐lived greenhouse gases: Calculations with the AER radiative transfer models. Journal of Geophysical Research: Atmospheres, 113(D13), https://doi.org/10.1029/2008JD009944, 2008.

Jin, Z. and Stamnes, K.: Radiative transfer in nonuniformly refracting layered media: atmosphere–ocean system. Applied Optics, 33(3), pp.431-442. https://doi.org/10.1364/AO.33.000431, 1994.

Kuipers Munneke, P., Van den Broeke, M.R., Lenaerts, J.T.M., Flanner, M.G., Gardner, A.S. and Van de Berg, W.J.: A new albedo parameterization for use in climate models over the Antarctic ice sheet. Journal of Geophysical Research: Atmospheres, 116(D5). https://doi.org/10.1029/2010JD015113, 2011

Lee, W.L. and Liou, K.N.: A coupled atmosphere–ocean radiative transfer system using the analytic four-stream approximation. Journal of the Atmospheric Sciences, 64(10), pp.3681-3694. https://doi.org/10.1175/JAS4004.1, 2007.

Liang, S., Fang, H., Chen, M., Shuey, C.J., Walthall, C., Daughtry, C., Morisette, J., Schaaf, C. and Strahler, A.: Validating MODIS land surface reflectance and albedo products: Methods and preliminary results. Remote sensing of environment, 83(1-2), pp.149-162. https://doi.org/10.1016/S0034-4257(02)00092-5, 2002.

Marshall, S. and Oglesby, R.J.: An improved snow hydrology for GCMs. Part 1: Snow cover fraction, albedo, grain size, and age. Climate Dynamics, 10(1-2), pp.21-37. https://doi.org/10.1007/BF00210334, 1994.

Marshall, S.E.: A Physical Parameterization of Snow Albedo for Use in Climate Models, NCAR Cooperative Thesis 123, National Center for Atmospheric Research, Boulder, CO, 175 pp. 1989.

Matzl, M. and Schneebeli, M.: Measuring specific surface area of snow by near-infrared photography. Journal of Glaciology, 52(179), pp.558-564. https://doi.org/10.3189/172756506781828412, 2006.

Matzl, M. and Schneebeli, M.: Stereological measurement of the specific surface area of seasonal snow types: Comparison to other methods, and implications for mm-scale vertical profiling. Cold Regions Science and Technology, 64(1), pp.1-8. https://doi.org/10.1016/j.coldregions.2010.06.006, 2010.

Meador, W.E. and Weaver, W.R.: Two-stream approximations to radiative transfer in planetary atmospheres: A unified description of existing methods and a new

The Cryosphere Discuss., https://doi.org/10.5194/tc-2019-22
Manuscript under review for journal The Cryosphere
Discussion started: 20 February 2019

improvement. Journal of the Atmospheric Sciences, 37(3), pp.630-643. https://doi.org/10.1175/1520-0469(1980)037<0630:TSATRT>2.0.CO;2, 1980.

Mlawer, E.J. and Clough, S.A.: On the extension of rapid radiative transfer model to the shortwave region. In Proceedings of the 6th Atmospheric Radiation Measurement (ARM) Science Team Meeting, US Department of Energy, CONF-9603149, 223–226. 1997.

Neale, Richard B., Chen, C.-C., Gettelman, A., Lauritzen, P. H., Park, S., Williamson, D. L., Conley, A. J., Garcia, R., Kinnison, D., Lamarque, J. F., and Marsh, D.: Description of the NCAR community atmosphere model (CAM 5.0). NCAR Tech. Note NCAR/TN-486+ STR 1, no. 1: 1-12. 2010.

Neshyba, S.P., Grenfell, T.C. and Warren, S.G.: Representation of a nonspherical ice particle by a collection of independent spheres for scattering and absorption of radiation: 2. Hexagonal columns and plates. Journal of Geophysical Research: Atmospheres, 108(D15). https://doi.org/10.1029/2002JD003302, 2003.

Perovich, D. K.: The optical properties of sea ice (No. MONO-96-1). COLD REGIONS RESEARCH AND ENGINEERING LAB HANOVER NH. 1996.

Stamnes, K., Tsay, S.C., Wiscombe, W. and Jayaweera, K.: Numerically stable algorithm for discrete-ordinate-method radiative transfer in multiple scattering and emitting layered media. Applied optics, 27(12), pp.2502-2509. https://doi.org/10.1364/AO.27.002502, 1988.

Thomas, G.E. and K. Stamnes (1999), Radiative transfer in the atmosphere and ocean. Cambridge University Press.

Toon, O. B., McKay, C. P., Ackerman, T. P., and Santhanam, K.: Rapid calculation of radiative heating rates and photodissociation rates in inhomogeneous multiple scattering atmospheres, J. Geophys. Res., 94(D13), 16,287–16,301. https://doi.org/10.1029/JD094iD13p16287, 1989.

Turner, A.K., Lipscomb, W.H., Hunke, E.C., Jacobsen, D.W., Jeffery, N., Ringler, T.D. and Wolfe, J.D.: MPAS-Seaice: a new variable resolution sea-ice model. J. Adv. Model Earth Sy., in preparation., 2018.

Wang, X., Doherty, S.J. and Huang, J.: Black carbon and other light‐absorbing impurities in snow across Northern China. Journal of Geophysical Research: Atmospheres, 118(3), pp.1471-1492. https://doi.org/10.1029/2012JD018291, 2013.

Warren, S. G.: Optical properties of snow. Reviews of Geophysics 20, no. 1: 67-89. https://doi.org/10.1029/RG020i001p00067,1982.

Warren, S.G. and Wiscombe, W.J.: A model for the spectral albedo of snow. II: Snow containing atmospheric aerosols. Journal of the Atmospheric Sciences, 37(12), pp.2734-2745.https://doi.org/10.1175/1520-0469(1980)037<2734:AMFTSA>2.0.CO;2, 1980

Warren, S.G. and Brandt, R.E.: Optical constants of ice from the ultraviolet to the microwave: A revised compilation. Journal of Geophysical Research: Atmospheres, 113(D14). https://doi.org/10.1029/2007JD009744, 2008.

The Cryosphere Discuss., https://doi.org/10.5194/tc-2019-22
Manuscript under review for journal The Cryosphere
Discussion started: 20 February 2019

The Cryosphere
Discussions
Open Access

Warren, S.G. and Wiscombe, W.J.: Dirty snow after nuclear war. Nature, 313(6002), p.467. https://doi.org/10.1038/313467a0, 1985.

Wiscombe, W. J.: The delta-Eddington approximation for a vertically inhomogeneous atmosphere, NCAR Tech. Note TN-140_STR [NTIS P6270618]. 1977.

Wiscombe, W.J.: Improved Mie scattering algorithms. Applied optics, 19(9), pp.1505-1509. https://doi.org/10.1364/AO.19.001505,1980.

Wiscombe, W.J. and Warren, S.G.: A model for the spectral albedo of snow. I: Pure snow. Journal of the Atmospheric Sciences, 37(12), pp.2712-2733. https://doi.org/10.1175/1520-0469(1980)037<2712:AMFTSA>2.0.CO;2, 1980.

Zender, C.S.: Global climatology of abundance and solar absorption of oxygen collision complexes. Journal of Geophysical Research: Atmospheres, 104(D20), pp.24471-24484. https://doi.org/10.1029/1999JD900797, 1999.

Zender, C.S., Bush, B., Pope, S.K., Bucholtz, A., Collins, W.D., Kiehl, J.T., Valero, F.P. and Vitko Jr, J.: Atmospheric absorption during the atmospheric radiation measurement (ARM) enhanced shortwave experiment (ARESE). Journal of Geophysical Research: Atmospheres, 102(D25), pp.29901-29915. https://doi.org/10.1029/97JD01781, 1997.

Figure 1. Spectral and total down-welling solar flux at surface computed using SWNB2 for (a) standard clear-sky and cloudy-sky atmospheric profiles of mid-latitude winter assuming solar zenith angle is 60° at the top of atmosphere, and for (b) standard clear sky profiles of mid-latitude and sub-Arctic winter with different incident solar zenith angles.

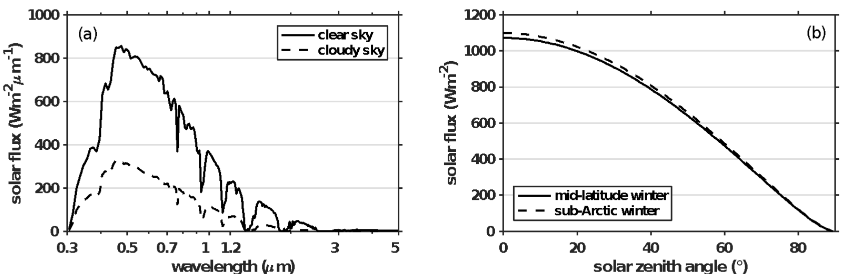

Figure 2. Spectral albedo of pure snow computed using 16-stream DISORT, SNICAR, CICE, and 2SD models, for clear-sky (direct beam at solar zenith angle 60°) and cloudy-sky conditions in the left and right panels, respectively. The top panels show spectral albedo. The middle panels show the difference ($\delta\alpha = \alpha_2 - \alpha_{16}$) in spectral albedos computed using 2-stream model (α_2) and 16-stream DISORT (α_{16}). The bottom panels show the different of reflected spectral flux given $\delta\alpha$. The snowpack is set to semi-infinite deep with grain radius of 100 μm.

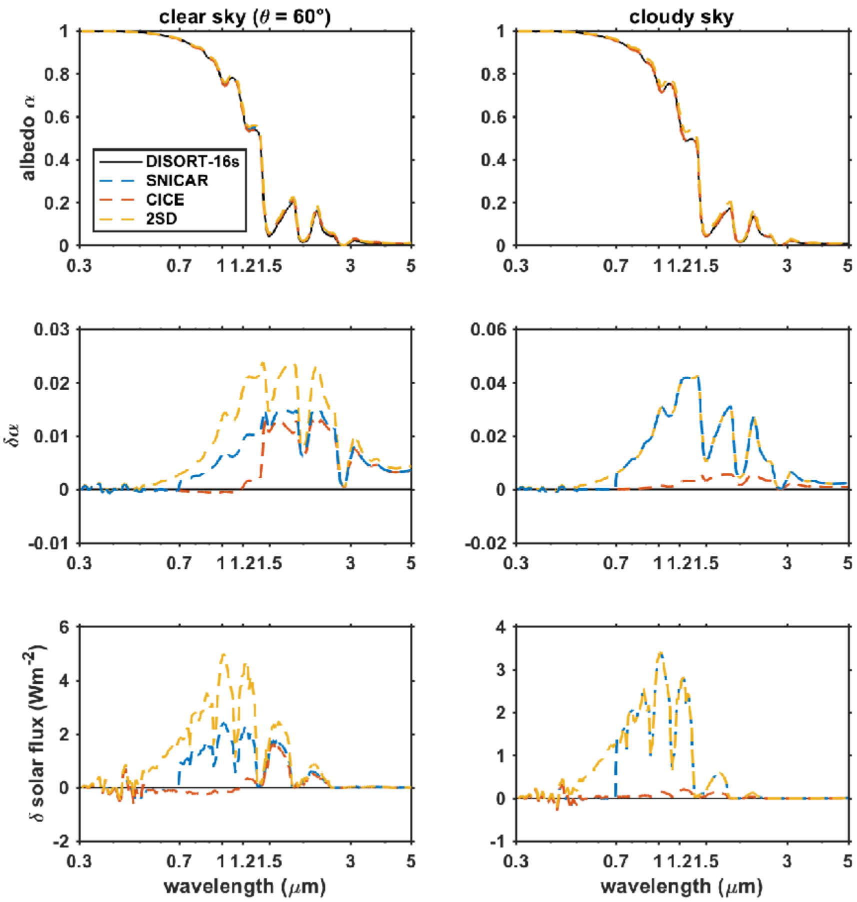

The Cryosphere Discuss., https://doi.org/10.5194/tc-2019-22
Manuscript under review for journal The Cryosphere
Discussion started: 20 February 2019

The Cryosphere Discussions
Open Access
EGU

Figure 3. The difference in direct snow albedo ($\delta\alpha = \alpha_2 - \alpha_{16}$) computed using 2-stream models (α_2) and using 16-stream DISORT model (α_{16}), for various snow depths and solar zenith angles, with snow gran radius of 100 µm. From the top to the bottom rows are results of 2-stream models SNICAR, CICE, and 2SD. From the left to the right columns are albedo differences of all-wave, visible, near-IR bands.

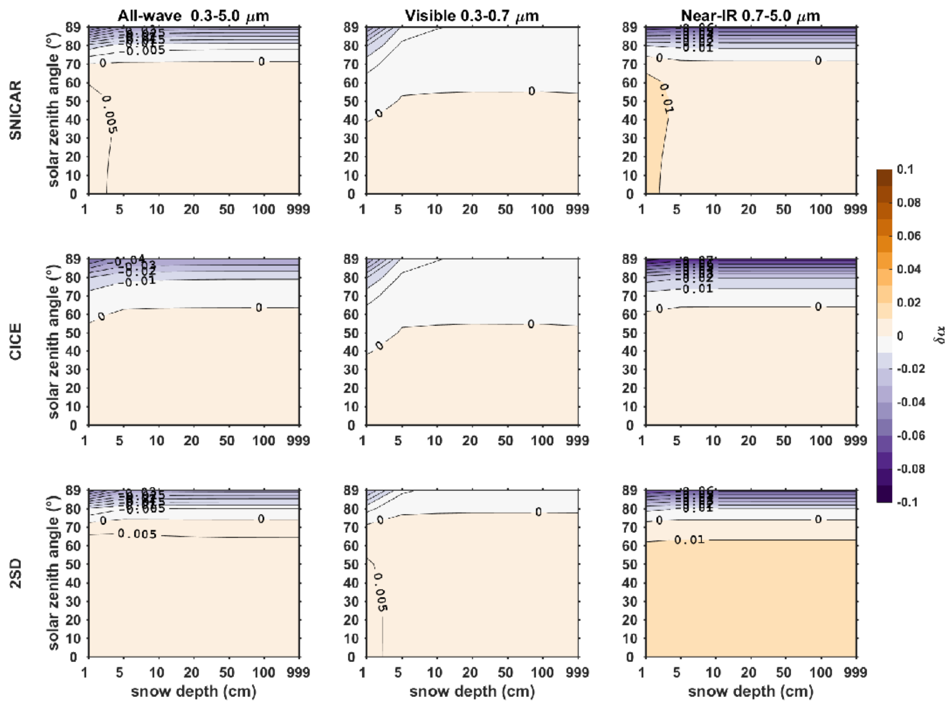

Figure 4. The same to Figure 3, but for snow grain radius of 1000 μm.

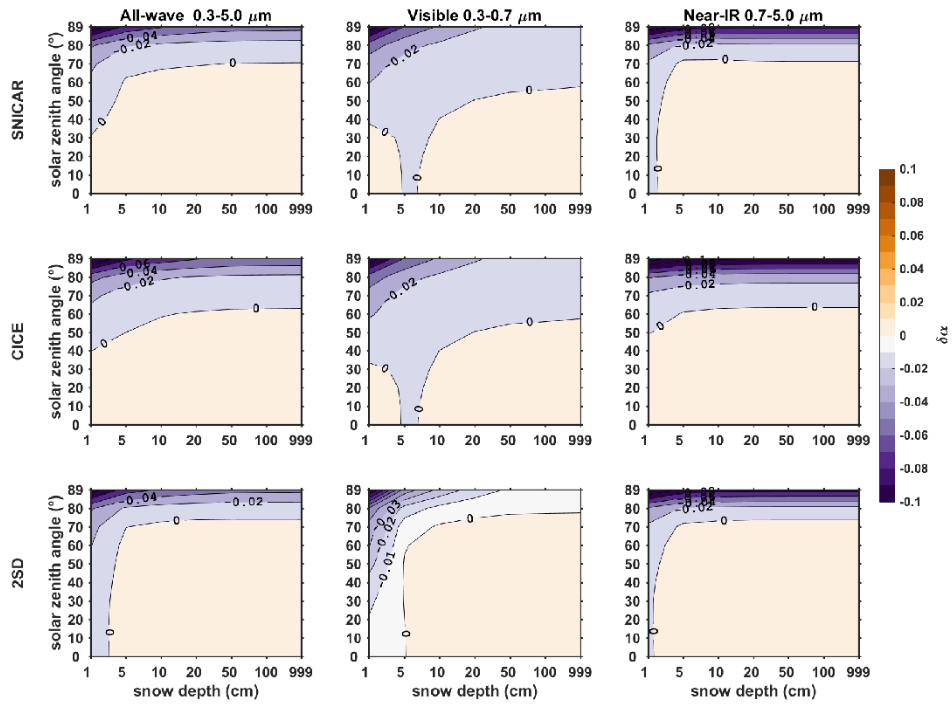

The Cryosphere Discuss., https://doi.org/10.5194/tc-2019-22
Manuscript under review for journal The Cryosphere
Discussion started: 20 February 2019

The Cryosphere
Discussions
Open Access

Figure 5. The same to Figure 3, but for fixed solar zenith angle of 60° and different snow grain radii.

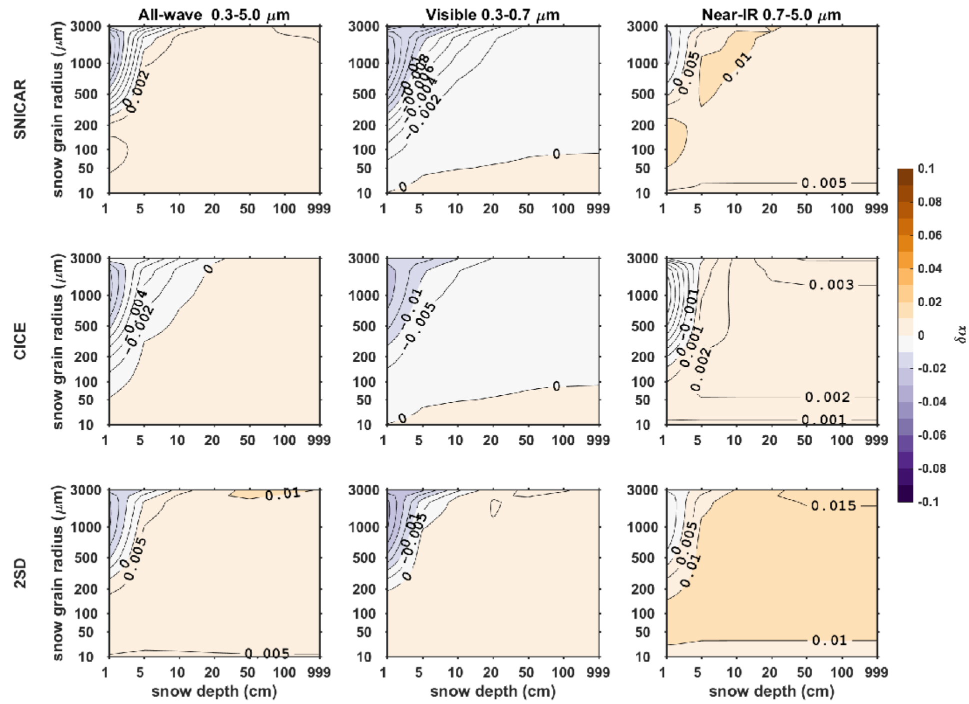

Figure 6. The same to Figure 5, but for diffuse snow albedo with different snow grain radii.

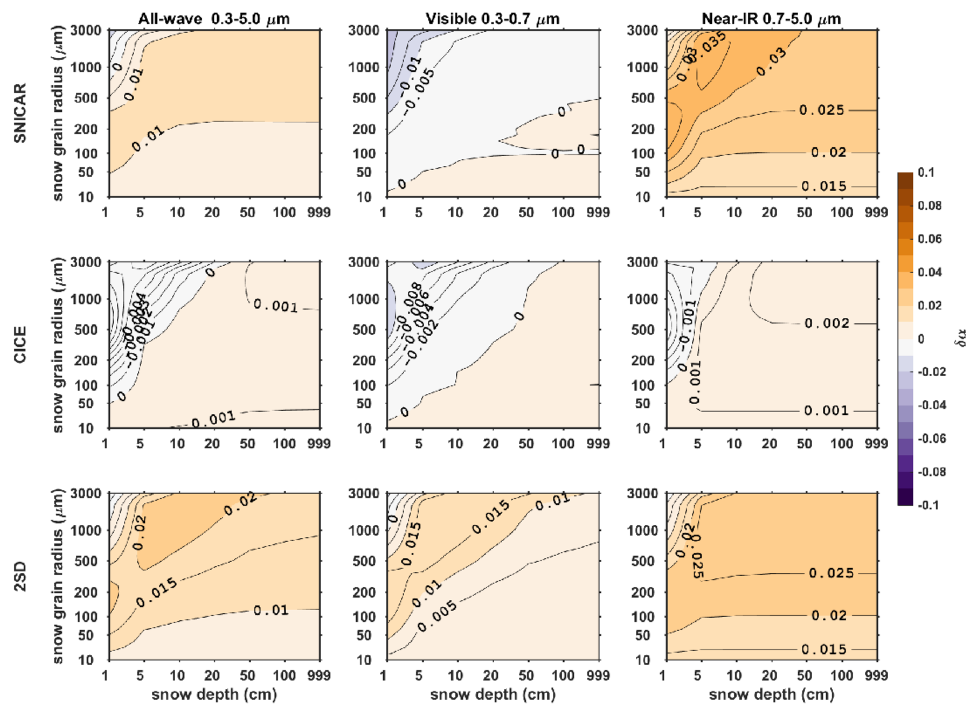

957 Figure 7. Error in reflected direct solar flux given albedo errors shown in Figure 3.

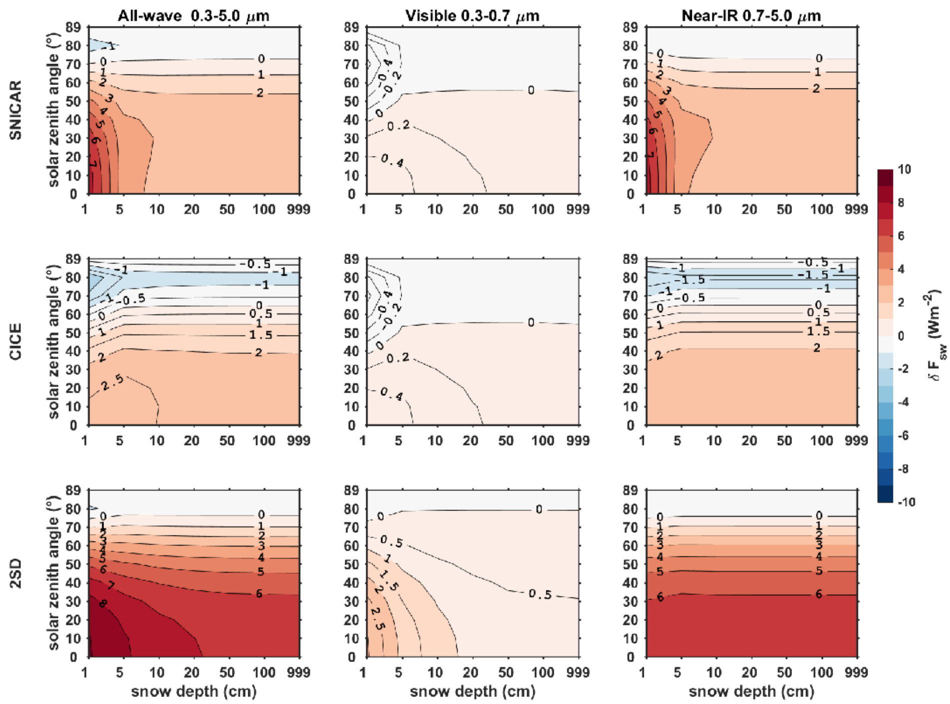

958
959

The Cryosphere Discuss., https://doi.org/10.5194/tc-2019-22
Manuscript under review for journal The Cryosphere
Discussion started: 20 February 2019

Figure 8. Error in reflected direct solar flux given albedo errors shown in Figure 4.

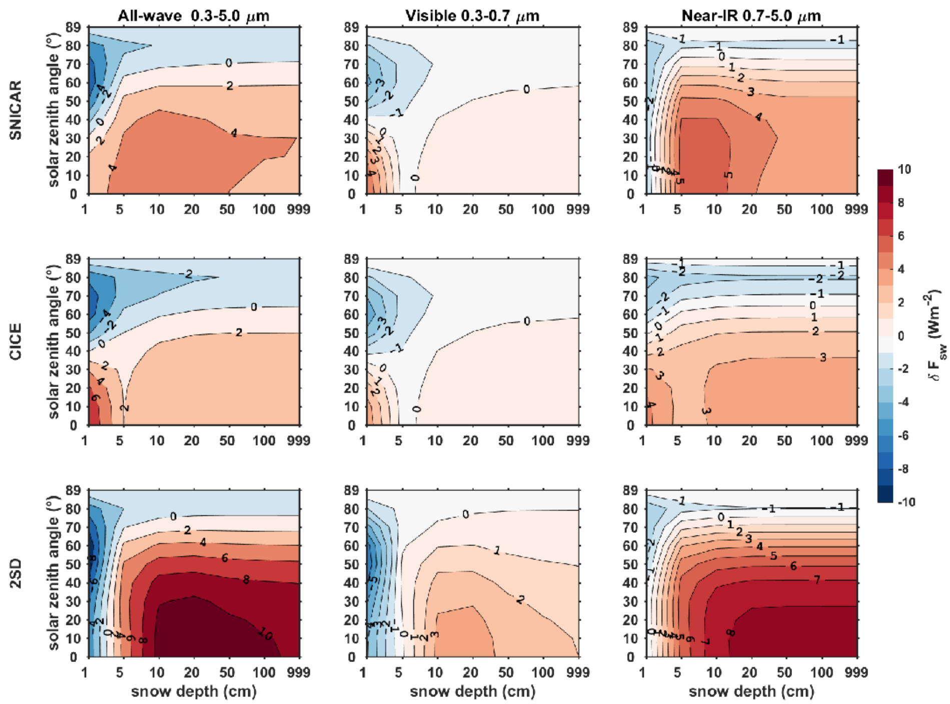

The Cryosphere Discuss., https://doi.org/10.5194/tc-2019-22
Manuscript under review for journal The Cryosphere
Discussion started: 20 February 2019

963 Figure 9. Error in reflected diffuse solar flux given albedo errors shown in Figure 6.

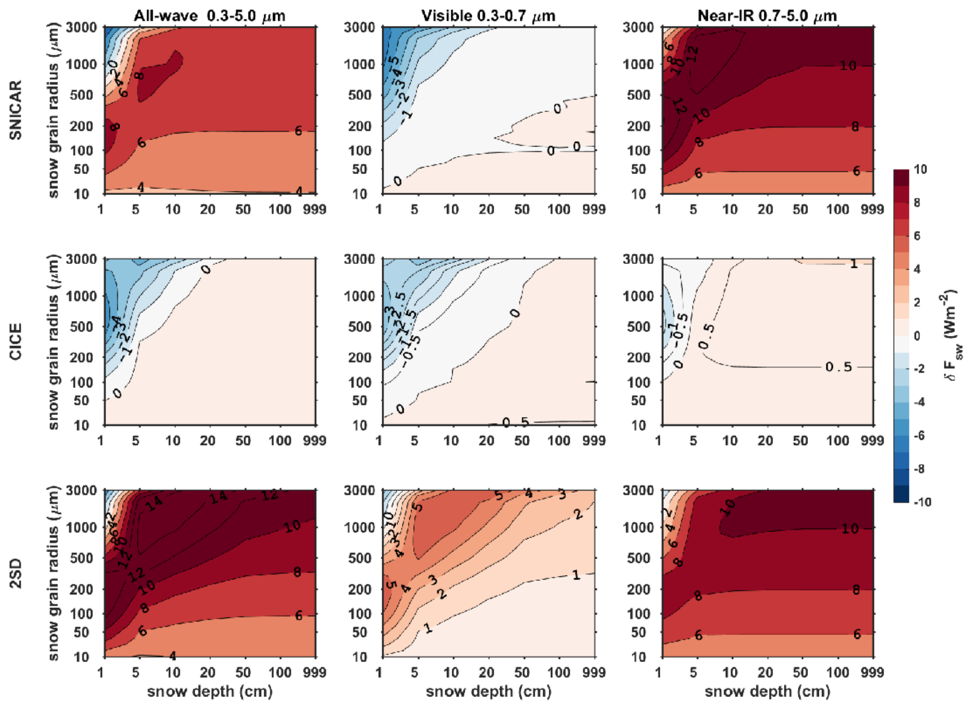

964
965
966

The Cryosphere Discuss., https://doi.org/10.5194/tc-2019-22
Manuscript under review for journal The Cryosphere
Discussion started: 20 February 2019

The Cryosphere
Discussions
Open Access

Figure 10. Comparison of light-absorption profiles derived from 2-stream models and 16-stream DISORT. The left-most column show fractional band absorptions computed using 16-stream DISORT. The right three panels show the errors of all-wave, visible, and near-IR fractional absorptions calculated using 2-stream models. The top and bottom panels are for clear-sky and cloudy-sky conditions (solar zenith angle of 60°), respectively. The snowpack is 10 cm deep, and is divided evenly into five 2-cm thick layers, for new snow (r = 100 μm) and old snow (r = 1000 μm). The layers 1-4 represent the top four snow layers (top 8 cm), and layer 5 represents underlying ground with albedo of 0.25.

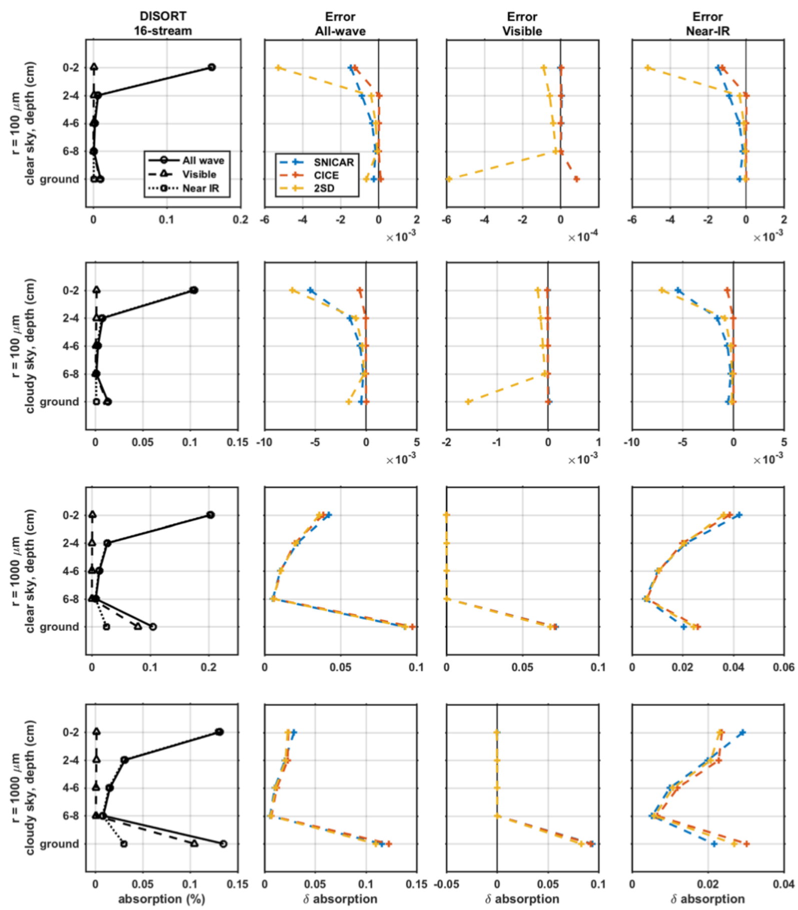

The Cryosphere Discuss., https://doi.org/10.5194/tc-2019-22
Manuscript under review for journal The Cryosphere
Discussion started: 20 February 2019

Figure 11. (a) Direct near-IR snow albedo and (b) near-IR fractional absorption by top 2-cm snow of a 2-m thick snowpack, for solar zenith angles larger than 70° and snow grain radii of 100 µm and 1000 µm. (c) The ratios of near-IR albedo computed using CICE to that computed using 16-stream DISORT for different solar zenith angles. These ratios are parameterized as liner functions of the logarithmic of snow grain radius. The slopes and y-intercepts are shown in (d). The black dashed curves in figures (c) and (d) are fitting values computed using parameterization discussed in Section 5.

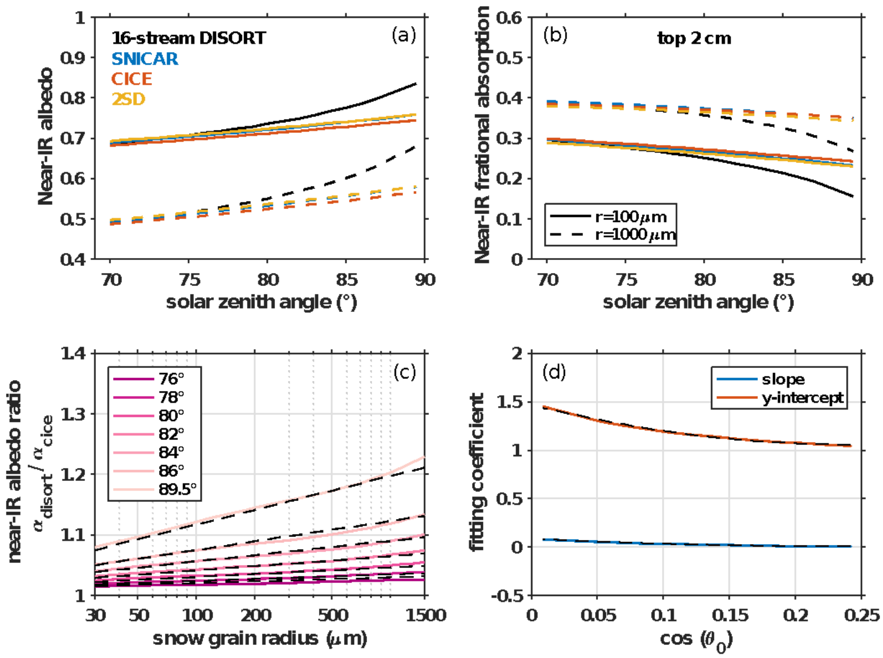

The Cryosphere Discuss., https://doi.org/10.5194/tc-2019-22
Manuscript under review for journal The Cryosphere
Discussion started: 20 February 2019

The Cryosphere
Discussions
Open Access

Figure 12. Error in semi-infinite snow albedo computed using CICE before (top row) and after (bottom row) incorporating corrections for near-IR albedo, for different solar zenith angles and snow grain radii.

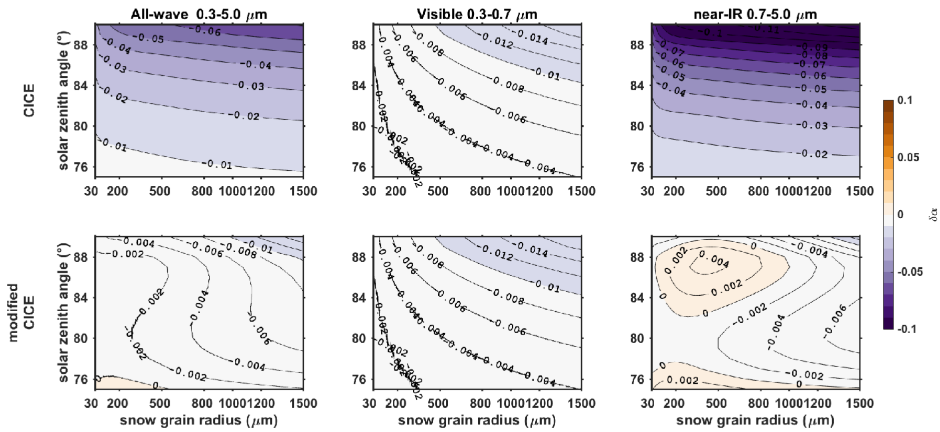

The Cryosphere Discuss., https://doi.org/10.5194/tc-2019-22
Manuscript under review for journal The Cryosphere
Discussion started: 20 February 2019

The Cryosphere Discussions

Table 1. Two-stream radiative transfer algorithms evaluated in this work, including algorithms that are currently implemented in Earth System Model CESM and E3SM.

ESM Component	Land	Sea Ice	
Model	SNICAR	CICE/MPAS-seaice	2SD
Radiative transfer approximation	2-stream δ-Eddington (visible) δ-Hemispheric-mean (near-IR)	2-stream δ-Eddington	2-stream δ-Discrete-ordinate
Treatment for multi-layered media	matrix inversion	adding-doubling	matrix inversion
Fresnel reflection/refraction	no	yes	yes
Number of bands implemented in ESMs	5 bands (1 visible, 4 near-IR)	3 bands (1 visible, 2 near-IR)	
Applies to	snow	bare/ponded/snow-covered sea ice, and snow	bare/ponded/snow-covered sea ice, and snow